UCRL 431
Cy. 2

UNIVERSITY OF CALIFORNIA

Radiation Laboratory

TWO-WEEK LOAN COPY

This is a Library Circulating Copy
which may be borrowed for two weeks.
For a personal retention copy, call
Tech. Info. Division, Ext. 5545

BERKELEY, CALIFORNIA

UCRL-431
c.2

DISCLAIMER

This document was prepared as an account of work sponsored by the United States Government. While this document is believed to contain correct information, neither the United States Government nor any agency thereof, nor the Regents of the University of California, nor any of their employees, makes any warranty, express or implied, or assumes any legal responsibility for the accuracy, completeness, or usefulness of any information, apparatus, product, or process disclosed, or represents that its use would not infringe privately owned rights. Reference herein to any specific commercial product, process, or service by its trade name, trademark, manufacturer, or otherwise, does not necessarily constitute or imply its endorsement, recommendation, or favoring by the United States Government or any agency thereof, or the Regents of the University of California. The views and opinions of authors expressed herein do not necessarily state or reflect those of the United States Government or any agency thereof or the Regents of the University of California.

UCRL-431
Unclassified Distribution

UNIVERSITY OF CALIFORNIA

Radiation Laboratory

UNCLASSIFIED

Contract No. W-7405-eng-48

Elastic Scattering of 84 Mev Neutrons

A. Bratenahl, S. Fernbach, R. H. Hildebrand,

C. E. Leith, and B. J. Moyer

August 25, 1949

Berkeley, California

Installation	No. of Copies
Argonne National Laboratory	8
Armed Forces Special Weapons Project	1
Atomic Energy Commission, Washington	2
Battelle Memorial Institute	1
Brookhaven National Laboratory	8
Bureau of Medicine and Surgery	1
Bureau of Ships	1
Carbide & Carbon Chemicals Corporation (K-25)	4
Carbide & Carbon Chemicals Corporation (Y-12)	4
Chicago Operations Office	1
Cleveland Area Office	1
Columbia University (Dunning)	1
Columbia University (Failla)	1
Dow Chemical Company	1
General Electric Company, Richland	6
Hanford Operations Office	1
Idaho Operations Office	1
Iowa State College	2
Kansas City	1
Kellex Corporation	2
Knolls Atomic Power Laboratory	4
Los Alamos	3
Mallinckrodt Chemical Works	1
Massachusetts Institute of Technology (Gaudin)	1
Massachusetts Institute of Technology (Kaufmann)	1
Mound Laboratory	3
National Advisory Committee for Aeronautics	2
National Bureau of Standards	2
Naval Radiological Defense Laboratory	2
NEPA Project	2
New Brunswick Laboratory	1
New York Operations Office	5
North American Aviation, Inc.	1
Oak Ridge National Laboratory	8
Patent Advisor, Washington	1
Rand Corporation	1
Sandia Base	1
Sylvania Electric Products, Inc.	1
Technical Information Branch, ORE	15
U. S. Public Health Service	1
UCLA Medical Research Laboratory (Warren)	1
University of California Radiation Laboratory	5
University of Rochester	2
University of Washington	1
Western Reserve University (Friedell)	2
Westinghouse	4
Total	119

Radiation Laboratory
University of California
Berkeley, California

Elastic Scattering of 84 Mev Neutrons

A. Bratenahl, S. Fernbach, R. H. Hildebrand

C. E. Leith, and B. J. Moyer

Radiation Laboratory, Department of Physics
University of California, Berkeley, California

August 25, 1949

Abstract

Measurements have been made of the angular distribution of 84 Mev neutrons scattered into angles between 2 1/2° and 25° by Al, Cu and Pb nuclei. Small spheres of these elements were placed in the neutron beam of the 184-in. cyclotron and the scattered neutrons with energies greater than 20 Mev were detected with pieces of carbon activated by the $C^{12}(n,2n)C^{11}$ reaction. Total scattering cross sections were obtained by integration of the differential scattering cross sections and also by attenuation measurements with good and poor geometry.

Elastic Scattering of 84 Mev Neutrons

A. Bratenahl, S. Fernbach, R. H. Hildebrand,

C. E. Leith, and B. J. Moyer

Radiation Laboratory, Department of Physics
University of California, Berkeley, California

August 25, 1949

I. Introduction

Amaldi *et al.*[1] have observed a portion of the elastic scattering pattern

(1) E. Amaldi, D. Bocciarelli, B. N. Cacciapuoti, and G. C. Trabacchi, Nuovo Cim. 3, 15-21 and 3, 203 (1946)

produced by 14 Mev neutrons incident on Pb nuclei. Using a relatively high intensity beam of 90 Mev neutrons from the 184-in. cyclotron the authors have explored the elastic scattering patterns of Al, Cu and Pb. The measurements were extended to small enough angles to include a large part of the distribution. By measuring the ratio of the scattered neutron flux to the flux incident on the scattering nuclei it was possible to determine the absolute differential scattering cross sections. Total scattering cross sections were obtained by integration of the differential cross sections. The total scattering cross sections were also measured directly by good and poor geometry attenuation experiments. It is of interest to compare these scattering cross sections to the total collision cross sections determined by Cook *et al.*[2] and by the

(2) L. J. Cook, E. M. McMillan, J. M. Peterson, and D. C. Sewell, Phys. Rev. 75, 7 (1949)

authors, using the same beam and the same detectors. This comparison provides a test of nuclear models such as the "opaque" model, and the "transparent" model of Fernbach, Serber, and Taylor.[3]

(3) S. Fernbach, R. Serber, and T. B. Taylor, Phys. Rev. 75, 1352 (1949)

II. General Features of the Experiment

The neutron source was a 1/2 in. thick beryllium target bombarded by 190 Mev deuterons in the 184-in. cyclotron. The energy distribution of neutrons from this source has a peak at 90 Mev and a spread at half maximum of 30 Mev.[4,5]

(4) J. Hadley, E. Kelly, C. Leith, E. Segrè, C. Wiegand and H. York, Phys. Rev. 75, 353 (1949)

(5) R. Serber, Phys. Rev. 72 1007 (1947)

The scattering experiment was performed in a narrow beam of neutrons defined by a circular hole in the 3 meter thick concrete shielding wall. (See Figure 1). The maximum beam intensity was about 10^6 neutrons per square centimeter per second. Some early experiments indicated that the flux density was essentially constant radially out to 4 cm from the axis of the beam and then decreased to less than 0.1 percent at 5 cm.

For the measurements of differential scattering cross sections the disposition of scatterer and detector is shown in Figure 1A. Spherical scatterers were used to simplify the determination of the effective scattering center and mean angle of scattering. The distance "r" was increased as θ was decreased so that the detector would not be in the beam. It was experimentally established that the activation of the detector at a given angle varied inversely as r^2 indicating freedom from unrecognized sources of detector activation.

The relative intensity of incident to scattered neutrons was measured by placing the detector in the position of the scatterer.

Two types of detection were employed in the course of the study. Most of the work was done with carbon detectors employing the (n,2n) reaction, but a coincidence recoil-proton counter was also used. Both receive discussion in subsequent sections.

The excitation function of the reaction $C^{12}(n,2n)C^{11}$ at high energies has

been investigated theoretically by Heckrotte and Wolff,[6] and experimentally by

(6) W. Heckrotte and Peter Wolff Phys. Rev. 73, 265 (1948)

R. L. Mather and H. F. York.[7] Using these results, and the known neutron

(7) R. L. Mather and H. F. York, Private Communication

energy distribution, the mean detection energy is determined to be 84 ± 4 Mev.

The activity of the carbon detectors was compared to the activity of a carbon monitor placed in the beam between the target and the scatterer. The monitor for the recoil proton detectors was a BF_3 slow neutron counter placed in a hole in the concrete shielding wall (Position B, Figure 1). Its response in this location was proportional to the high energy neutron flux incident upon the shielding in the region of collimation.

The measurements of total cross sections and absorption cross sections were obtained simultaneously with the arrangement shown in Figure 2. The attenuation measured by this detector gives a cross section for removal of detectable neutron flux from a forward cone extending to the maximum angle, θ_m, subtended by the absorber about the detector. This angle is chosen to be the same as the maximum angle at which differential scattering cross sections were measured, and it includes essentially all of the elastically scattered neutrons. The cross section obtained in this manner is thus approximately equal to the absorption cross section. A further discussion of this measurement will be found in Section III-B. A good geometry detector shielded from all but the central portion of the absorber was used to measure the total cross section simultaneously.

III. Analysis and Description of the Experiment

A. Angular Distribution

1. Analysis. - Neglecting absorption of the neutrons passing through the scatterer, the activation of a detector of area S placed at angle θ and distance r from the scatterer of volume V is given by

$$D(r,\theta) = \left(I_0 \frac{N_0 \rho}{A} V\right)\left(\sigma(\theta)\frac{S}{r^2}\right)\eta , \qquad (1)$$

where

I_0 = incident intensity,

$\frac{N_0 \rho}{A} V$ = number of scattering nuclei,

$\sigma(\theta)$ = cross section for scattering into unit solid angle at angle θ,

$\frac{S}{r^2}$ = solid angle subtended by the detector, and

η = efficiency of the detector.

If the detector is placed in the neutron beam the activation is given by

$$D_0 = I_0 S \eta . \qquad (2)$$

Thus from (1) and (2)

$$\sigma(\theta) = \frac{D(r,\theta)}{D_0}\frac{Ar^2}{N_0 \rho V} . \qquad (3)$$

Taking absorption and multiple scattering into account a formula is obtained which is the same as (3) multiplied by a constant depending on the radius of the scattering sphere and the total and absorption cross sections.

The method employed in finding the complete expression may be outlined as follows.

A representation of the intensity and angular distribution of the neutrons scattered by a slab of thickness x may be given in the form

$$I(\theta) = I_0 \sum_{n=1}^{\infty} \left\{\left[\frac{1}{n!}(x\mu_s)^n \exp.(-x\mu_t)\right]\left[\frac{1}{n\sigma_s}\sigma\left(\frac{\theta}{\sqrt{n}}\right)\right]\right\} ,$$

where

$I(\theta)$ = flux per unit solid angle in direction θ,

μ_t, μ_s = attenuation constant for collision, and for elastic scattering, respectively,

σ_s = cross section for elastic scattering.

The first factor of a typical "nth" term gives the probability of just n elastic scattering collisions, and no other collisions, in passing through the slab. Deviations are assumed sufficiently small that the distance traversed in the material is always x.

In the second factor, giving the probability that an n-times-scattered neutron goes in direction θ, the customary assumption has been made that the angular spread after n scatterings is $\sqrt{n}$ times the spread from single scattering. This implies that the forward scattered intensity shall be correspondingly reduced by the factor 1/n.

When this type of analysis is applied to the scattering by the spheres used (such as, copper, 2.5 cm diam.), it is found that the coefficient multiplying $\sigma\left(\frac{\theta}{\sqrt{2}}\right)$ is only 5 percent of the coefficient of $\sigma\left(\frac{\theta}{\sqrt{1}}\right)$. Hence the effect of multiple scattering upon the <u>form</u> of the angular distribution from such a sphere is not sufficiently serious to demand attention in treating data of the present accuracy; and it is necessary only to correct for the effects of absorption and multiple scattering in an integral manner rather than to evaluate a correction which depends upon angle.

Having recognized this, it is found to be convenient to evaluate the correction by the following type of analysis. In traversing a slab of thickness x a neutron will have a probability $[1-\exp.(-x\mu_s)]$ of being elastically scattered, and a probability $\exp.(-x\mu_a)$ of emerging without an inelastic collision; where μ_a is the attenuation constant for an inelastic or absorbing collision. Since $\mu_t = \mu_a + \mu_s$, the product of these probabilities is $\exp.(-x\mu_a)-\exp.(-x\mu_t)$.

Applying this to a spherical scatterer of radius <u>a</u>, the expression for the activation of the detector at angle θ and distance r becomes

$$D(r,\theta) = D_0 \frac{1}{\sigma_s} \sigma \quad (\theta) \frac{1}{r^2} \int_s [\exp.(-x\mu_a)-\exp.(-x\mu_t)] \, ds ,$$

where the integration is carried out over the cross sectional area of the

scatterer. The variable x is the length of the chord which is used to approximate the neutron path.

Evaluation of the integral and series expansion results in the equation:

$$D(r,\theta) = D_0\left(\frac{N_0\rho}{A}V\right)\sigma(\theta)\frac{1}{r^2}K ,$$

where

$$K = 1 - \frac{3}{4}a(\mu_t + \mu_a) + \frac{2}{5}a^2(\mu_t^2 + \mu_t\mu_a + \mu_a^2)$$
$$- \frac{1}{6}a^3(\mu_t^3 + \mu_t^2\mu_a + \mu_t\mu_a^2 + \mu_a^3) + \ldots$$

Solving for $\sigma(\theta)$ we have instead of (3):

$$\sigma(\theta) = \frac{D(r,\theta)}{D_0}\frac{Ar^2}{N_0\rho V}\frac{1}{K} \qquad (4)$$

2. Apparatus and Experimental Procedure. - The scatterers used were 2.54 cm diameter spheres of lead and copper and a 3.81 cm diameter sphere of aluminum. These were suspended in the beam by fine wires. The size of the scatterers was limited to keep the self-attenuation factor K from becoming less than 0.75.

The detectors were stacks of twelve cylindrical sectors of carbon 0.32 cm thick in a copper container (See Figure 3A). Two such stacks were placed symmetrically about the axis of the beam at distances, depending upon angle, of 18 to 125 cm. The wall of the copper container which faces the scatterer was made 1 cm thick to prevent activation of the carbon pieces by scattered protons. When this thickness was doubled the activity was reduced by the fraction which one would expect if all the activity were due to neutrons. After a 15 minute bombardment at the maximum cyclotron beam intensity the carbon sectors were removed from the copper holders and arranged to surround a set of four thin-glass-walled counting tubes (See Figure 3B).

The monitors were carbon discs of 4.29 cm diameter and 0.32 cm thickness. These were counted with a mica window bell-jar type counter. All counts were

made concurrently; that is, the detector and monitor activities were counted over the same time interval eliminating the necessity of corrections for decay.

In all the experiments described here the basic measurement is the ratio of the activity of the detector to that of the monitor. Calling this ratio A, when the scattering sphere is in place and the detector at (r,θ) (See Figure 1A); and B, the background ratio when the scatterer is removed but the detector is put in the same position; and C, the ratio when the detector is put in the primary beam in place of the scatterer, we have:

$$D(r,\theta) = (A - B)e$$

$$D_0 = 2Ce$$

where e is a relative counting tube efficiency factor to allow the results of different runs to be correlated, and $D(r,\theta)$ and D_0 are the quantities to be used in Equation (4). The value of e is determined before each run by counting arbitrary fixed samples with the detector and monitor counters. The factor 2 in the second equation above is necessary because only one of the copper holders was placed in the beam.

A typical determination of A involved about 2500 net counts from the detector in a period of 15 minutes. This is about four times the counter background for the set of four tubes used and about four times the net count in determining B. Since the monitor was exposed in the primary beam it gave a much higher count. The ratio $D(r,\theta)/D_0$ was of the order of 0.001.

B. Attenuation Experiments

1. Analysis. - From the results of the angular distribution measurements one can determine by graphical integration the cross section σ_s' for scattering of detectable neutron flux into a forward cone extending to the widest angle measured θ_m:

$$\sigma_s' = \int_0^{2\pi} d\Phi \int_0^{\theta_m} \sigma(\theta) \sin\theta d\theta \qquad (5)$$

This cross section can also be measured in an attenuation experiment utilizing

the "poor geometry" arrangement of Figure 4 in which the attenuating material forms the frustum of height x of a cone whose generating angle is θ_m.

For this arrangement the detectable neutron intensity at the detector when the attenuator thickness is x will be

$$I(x) = I_1(x) + 2\pi \int_0^{\theta_m} \sin\theta \, I(\theta,x)d\theta \; ; \tag{6}$$

where $I_1(x)$ is the flux density of unscattered neutrons at a distance x from the base and $I(\theta,x)$ is the intensity at x of previously scattered neutrons moving in direction θ within unit solid angle. This assumes that any increase due to detection of inelastically scattered neutrons is small, as will be justified in Section V.

Consider now the effect of increasing the thickness of the attenuating material by an amount dx. The intensity of detectable neutrons at the vertex of the cone will then be altered by an amount

$$\begin{aligned} dI(x) = &- I_1(x)N\sigma_t dx - 2\pi N\sigma_t dx \int_0^{\theta_m} \tan\theta \, I(\theta,x)d\theta \\ &+ 2\pi I_1(x)Ndx \int_0^{\theta_m} \tan\theta \, \sigma(\theta)d\theta \\ &+ 2\pi Ndx \int_0^{\theta_m} \tan\theta d\theta \int_0^{\alpha_m} \sigma(\beta)2\pi \sin\alpha \, I(\alpha,x)d\alpha \; . \end{aligned} \tag{7}$$

where N is the number of nuclei per cm^3 in the attenuator, and σ_t is the total cross section of each nucleus.

The physical meanings of the successive terms on the right-hand side of this equation are as follows:

1. Decrease due to attenuation in dx of hitherto unscattered neutrons whose flux density is $I_1(x)$.
2. Decrease due to attenuation in dx of neutrons previously elastically scattered into the direction of the detector.
3. Increase due to elastic scattering in dx, into the direction of the

detector, of hitherto undeviated neutrons.

4. Increase due to elastic scattering in dx of neutrons previously elastically scattered. The angle β defines the scattering angle necessary to deflect these incident neutrons into the direction of the detector. The angle α_m is to be large enough to include essentially all the elastically scattered flux incident upon dx.

Since $\sigma(\theta)$ and $I(\theta)$ are both strongly peaked at $\theta = 0$ the integrals in (7) are not greatly affected by replacing $\tan\theta$ by $\sin\theta$. (In the worst case the difference is only 2.5 percent.) Also for the same reason it may be shown that the angle β may be replaced by θ with an error sufficiently small to be allowable in this experiment. These two approximations are, in fact, partially compensating in their effects.

In view of Equations (6) and (5), these approximations permit (7) to be reduced to

$$dI(x) = - I(x)N(\sigma_t - \sigma_s')dx \; ;$$

so that an attenuation experiment with this arrangement will measure the difference of cross sections

$$\sigma_t - \sigma_s' = \frac{1}{Nx} \ln \frac{I_0}{I(x)} \; . \qquad (8)$$

The absorption cross section for the nuclei of the attenuating material is related to (8) by

$$\sigma_a = \sigma_t - \sigma_s' - \sigma_1 + \sigma_2 \; , \qquad (9)$$

where σ_1 accounts for elastic scattering into angles greater than θ_m, and σ_2 is the cross section for inelastic scattering of neutrons into angles less than θ_m with sufficient energy to be detected.

Subtraction of the quantity $(\sigma_t - \sigma_s')$ from the measured value of σ_t yields an evaluation of σ_s'

$$\sigma_s' = \sigma_t - (\sigma_t - \sigma_s') \qquad (10)$$

which may be compared for consistency with that obtained by Equation (5). If as is shown in Section V the quantities σ_1 and σ_2 are small, then σ_s' is approximately equal to the elastic scattering cross section $\sigma_s = \sigma_t - \sigma_a$.

2. Apparatus and Experimental Procedure. - The arrangment for the attenuation experiment just discussed is shown in Figure 2.

The angle θ_m was 27° for dural and copper, and 21° for lead. The maximum attenuator thicknesses were as follows: dural and copper, six 5.08 cm discs; lead, six 2.54 cm discs. In every case a 4 cm lead shield was put just ahead of the poor geometry detector to avoid activation of the carbon by recoil protons from the attenuating material. The uniformity of the incident beam was checked in a preliminary experiment by putting carbon detectors at various points on the base of the absorbing cone. This was also checked by verifying that a single disc at the base of the cone gave the same attenuation as a disc of the same thickness near the vertex. Absorption and total cross sections for aluminum were obtained from the dural measurements making allowance for the other metals in the alloy.

IV. Results

The results are summarized in Tables I and II and Figure 5.

Table I

Total cross sections and the cross sections σ_s' (See Section III-B1) in units of 10^{-24} cm^2. The third row of the Table gives scattering cross sections obtained from the total and absorption cross sections using Equation (10). The last row gives the scattering cross section obtained by integration of the differential cross section as in Equation (5).

Element	Al	Cu	Pb
Total cross sections			
Cook et al[2]	1.12 ± 0.02	2.22 ± 0.04	4.53 ± 0.09
The authors	1.14 ± 0.03	2.15 ± 0.04	4.47 ± 0.11
σ_s'			
By attenuation	0.65 ± 0.04	1.32 ± 0.03	2.64 ± 0.08
By integration	0.71 ± 0.04	1.37 ± 0.07	2.79 ± 0.14
Maximum angle θ_m	27°	27°	21°

Table II

Differential cross section in units of 10^{-24} cm^2 per steradian. The errors shown apply to the relative magnitudes and do not include a 3 percent error in assigning absolute magnitudes.

Angle in Degrees	Al	Cu	Pb
2 1/2	5.0 ± 0.4	13.8 ± 0.9	59. ± 4.
3		14.8 ± 1.2	54. ± 6.
4	4.64 ± 0.18	14.2 ± 0.7	53. ± 5.
5	4.36 ± 0.23	10.3 ± 0.3	34. ± 7.
6	4.3 ± 0.3	10.6 ± 0.3	25.6 ± 1.0
7 1/2	3.30 ± 0.15	7.34 ± 0.22	11.3 ± 1.1
10	2.24 ± 0.15	4.66 ± 0.07	4.3 ± 0.6
12 1/2	1.54 ± 0.13	2.61 ± 0.05	2.1 ± 0.3
15	1.08 ± 0.04	1.30 ± 0.02	1.46 ± 0.14
17 1/2	0.66 ± 0.07	0.53 ± 0.03	1.58 ± 0.11
20	0.38 ± 0.02	0.40 ± 0.03	1.04 ± 0.10
22 1/2			0.59 ± 0.13
25	0.17 ± 0.02	0.31 ± .05	

V. Sources of Error

A. Angular Resolution

Because of the finite size of the scatterer and detector a measurement made at a given nominal angle actually corresponds to detection over a fairly wide range of angles as is shown in Figure 6. A detailed analysis has shown that the errors of the angles and cross sections due to this effect are negligible considering the accuracy of the experiment. This effect alone would not prevent the detection of a minimum of the type theoretically predicted for diffraction by an opaque nucleus.

B. Detection of Inelastically Scattered Neutrons

The 20 Mev threshold of the $C^{12}(n,2n)C^{11}$ reaction made it quite possible that a part of the scattered flux detected in this experiment was due to inelastically scattered neutrons with energies greater than the 20 Mev detection threshold. For this reason the angular distributions were also measured using a recoil proton detector with a BF_3 slow neutron counter as a monitor (See Section II). The detector consisted of a 3.8 cm diameter, 5 cm long paraffin

cylinder behind which was placed a set of three cylindrical proportional counters each 5 cm in diameter and 5 cm long which were used in coincidence. A copper absorber was placed between the second and third counter. Its thickness was such that only recoil protons from neutrons with energies greater than 60 Mev could be detected; thus, as a neutron detector this arrangment provided a 60 Mev detection threshold.

Attenuation measurements, made with this detector and monitor combination indicated that under the conditions of operation, it was less reliable than the carbon detectors particularly for the measurement of the very small ratio $D(r,\theta)/D_0$. However, within the accuracy of the measurements the differential cross sections measured by the two methods are in agreement as can be seen in Figure 5.

The contribution of inelastic scattering is not large enough to be apparent in comparing the results of the two methods.

An estimate of the inelastic contribution can, however, be obtained from measurements of Hadley and York[8] on the differential cross sections of several

---

(8) J. Hadley, H. F. York, To be published

---

elements for production of high energy secondary protons by 90 Mev neutrons. At these energies the incident neutron wave length is sufficiently small to allow the effects of neutron-nucleon collisions to be observed, where the collision event involves primarily only the incident neutron and a neutron or proton of a target nucleus. By this process nucleons may be knocked out of nuclei with energies and angular distributions corresponding to those of n-p or n-n collisions.

Hadley and York have measured differential cross sections for such emission of protons of over 20 Mev energy from C, Cu, and Pb. We shall assume that the neutrons emerging from n-p collisions within the nucleus are described by the same differential cross section as these protons.

There will also be a contribution of high-energy neutrons due to n-n collisions. We assume that these events are similar to p-p collisions with respect to

cross section and angular distribution. Observations in progress at this laboratory indicate that even at these energies the p-p collisions yield spherical symmetry in the center-of-mass system, and that the collision cross section at these energies is roughly one-half the n-p collision cross section.

Using these assumptions, and taking account of the relative numbers of neutrons to protons in the nucleus in question, cross sections σ_2 of the target nuclei for delivering detectable neutrons by these "knock-on" processes into the angular range detected have been calculated and are shown in the Table III.

DeJuren and Knable[9] have measured total cross sections and the cross

(9) J. DeJuren and N. Knable, to be published

sections for scattering of detectable flux into angles less than θ_m using the same absorbers as those used by the authors. In place of carbon detectors they used bismuth fission chambers for which the neutron counting threshold is about 50 Mev, and the mean detection energy for these neutrons is about 95 Mev. Because of the higher threshold of this detector it is to be expected that the cross sections σ_s' as measured by DeJuren and Knable include smaller contributions from inelastic scattering than the corresponding cross sections measured by the authors. The ratios σ_s'/σ_t and $(\sigma_s' - \sigma_2)/\sigma_t$ from the carbon detector measurements and the ratio σ_s'/σ_t from bismuth fission detector measurements are shown in Table III. Considering this comparison, and the similarity of the angular distributions observed using proportional counters with the 60 Mev threshold with those observed with carbon detectors, it appears likely that these cross sections for inelastic processes yielding detectable neutrons are not underestimated.

In order to estimate the true scattering cross section σ_s one must add the effect of the cross section σ_1 for elastic scattering into wide angles which will be discussed in the next section.

Thus: $\sigma_s = \sigma_s' - \sigma_2 + \sigma_1$

Hence the values $\sigma_s' - \sigma_2$ of Table III represent lower limits for σ_s.

Table III

Observed scattering cross sections σ_s', calculated cross sections σ_2 for producing detectable neutrons by inelastic collisions, and comparisons of ratios of cross sections measured at two energies. (Cross sections in units of 10^{-24} cm^2.)

	Al	Cu	Pb
Observed scattering cross sections σ_s'	0.71	1.37	2.79
Calculated values of σ_2	0.07	0.13	0.17
$(\sigma_s' - \sigma_2)$	0.64	1.24	2.62
σ_s'/σ_t	0.62	0.64	0.62
$(\sigma_s' - \sigma_2)/\sigma_t$	0.56	0.58	0.59
σ_s'/σ_t, measured with Bi fission counters (~95 Mev)	0.58	0.61	0.60

Rann

C. Elastic Scattering into Wide Angles

The neutron flux per unit solid angle becomes so small at angles greater than θ_m that measurements of the intensity become very inaccurate. However, because of the sine factor which enters into the calculation of the scattering cross sections (See Equation (5)) the total flux in wide angles may not be negligible. An indication of the order of magnitude of this effect can be obtained from wide angle differential cross section measurements made with the recoil proton detector.

At 30° the differential cross sections measured were .033 ± .020, .004 ± .004, and .22 ± .13 for Al, Cu and Pb respectively. At 45° the value obtained for aluminum was .004 ± .001 while no flux was detected at this angle from Cu and Pb and no flux was detected in measurements at 60° and 90° from Pb. On the basis of these observations it has been estimated that the wide angle scattering effect is of the order of 5 percent for Al and less than this for Cu and Pb and is thus somewhat smaller than the inelastic scattering effect. As can be seen from Equation (9) the two effects tend to cancel each other in the evlauation of the difference between σ_s' and the true elastic scattering cross section σ_s.

It should be noticed that these effects are common to both methods of measuring σ_s, hece the attenuation method serves principally as a check on other systematic errors in the differential cross section measurements.

VI. Analysis of Results

A. Description of the Angular Distribution

In the present experiment the DeBroglie wave length of the neutrons is smaller than nuclear dimensions, and it is sensible to speak of a neutron colliding within the area of cross section presented by the nucleus. This implies that neutrons with rather large values of angular momentum will be involved in nuclear collisions.

The quantized values of angular momentum will extend up to $pR = \ell\hbar$ or $\ell = kR$; where $k = 1/\lambda\!\!\!^{-} = p/\hbar$, and ℓ is an angular momentum quantum number. R is the largest value of impact parameter for which observable effects of collision occur, and it may be defined as the nuclear radius.

For 84 Mev neutrons $\lambda\!\!\!^{-} = 0.48 \times 10^{-13}$ cm, and for a heavy nucleus R is nearly 10^{-12} cm. Thus values of ℓ will in some cases extend nearly as high as 20.

Since at the degree of excitation which such neutrons could impart to nuclei the nuclear levels will be numerous and overlapping, it is to be expected that such collisions would lead to inelastic events or absorption. Inelastically scattered neutrons or secondary neutrons from such events are almost entirely of energies below the detection threshold as indicated in Section V. Thus it is possible to conceive of the nucleus, for the purpose of this experiment, as an opaque, spherical obstacle absorbing and diffracting the neutron wave.

If a description of the scattering process is represented in partial waves,[10]

---

(10) Rayleigh, J. W. Strutt, Proc. Lond. Math. Soc. (1) IV, 253 (1873)

---

and the expression for the scattered wave obtained by subtracting the expression for the unperturbed plane wave from that for the wave field with scattering

nucleus present, the assymptotic result at a large distance r from the scattering center, and at angle θ from the direction of the incident beam, is:

$$\Psi_{scatt.} \simeq \frac{e^{ikr}}{2ikr} \sum_{\ell=0}^{\infty} (2\ell + 1) \left(e^{2i\delta_\ell} - 1\right) P_\ell (\cos\theta) \qquad (11)$$

When no absorption in the scattering nucleus occurs, δ_ℓ is a real number which measures the phase difference between the ℓth partial wave in the diverging components of the actual wave field and the corresponding wave in the unperturbed field. But when the scattering nucleus also absorbs neutrons the effect is described by a complex value for δ_ℓ,

$$\delta_\ell = \xi_\ell + i\eta_\ell ,$$

where η_ℓ then functions as an absorption exponent affecting the magnitude of the diverging ℓ^{th} wave.

If now the scattering nucleus is considered to be a perfectly absorbing sphere of radius R, the value of η_ℓ for $0 \leq \ell \leq kR$ will be infinite. Also if neutrons passing with $\ell > kR$ are to be unaffected the value of δ_ℓ will be zero for $\ell > kR$.

For this approximate model, then, the scattered wave (11) reduces to:[11, 12]

(11) G. Placzek and H. Bethe, Phys. Rev. 57, 1075A (1940)

(12) A. Akhieser and I. Pomeranchuk, J. Phys., U.S.S.R. IX, 471 (1945)

$$\Psi_{scatt.} \simeq - \frac{e^{ikr}}{2ikr} \sum_{\ell=0}^{\ell=Kr} (2\ell + 1) P_\ell (\cos\theta) \qquad (12)$$

The result (12) can be directly obtained by noting that the effect of the nucleus is to remove from the diverging components of the unperturbed wave those partial waves with values of ℓ up to $\ell = kR$. This removal is mathematically described by superimposing upon the unperturbed wave a set of partial waves with amplitudes equal to corresponding amplitudes of the unperturbed wave field, with values of ℓ up to $\ell = kR$, and with each phase shifted by one-half cycle. This superimposed set represents the scattered neutrons and its expression is just

(12). This is simply an application of Babinet's principle from physical optics.

From (12) the differential scattering cross section is seen to be

$$\sigma(\theta) = \frac{1}{4k^2}\left[\sum_{\ell=0}^{\ell=kR} (2\ell - 1)\, P_\ell\, (\cos\theta)\right]^2 \tag{13}$$

For forward scattering, $\theta = 0$, (13) yeilds

$$\sigma(0^\circ) = \frac{1}{4} k^2 \left(R + \frac{1}{k}\right)^4 \tag{14}$$

It is to be expected that the opaque nucleus model should give a distribution of elastically scattered neutrons similar to the Fraunhofer diffraction pattern for a plane wave diffracted by an opaque circular disc. It can be shown that expression (13) can be written in the approximate form[11,12]

$$\sigma(\theta) = \frac{1}{4} k^2 (R')^4 \left[\frac{J_1(2kR' \sin\frac{\theta}{2})}{kR' \sin\frac{\theta}{2}}\right]^2 \tag{15}$$

where J_1 indicates a first order Bessel Function, and $R' = R + \frac{1}{k}$. This is the expression for intensity in the Fraunhofer pattern produced by a disc of radius R' diffracting plane waves with $\lambda\!\!\!^{-} = 1/k$.

B. Effect of Neutron Energy Spread Upon Angular Distribution

The energy dependence of the differential cross section occurs through the quantity $k = \frac{1}{\lambda\!\!\!^{-}} = p/\hbar$. In order to compare the theoretical distribution (13) with one observed it is necessary to calculate from (13) or (15) a predicted value of $\sigma(\theta)$ by averaging over the energy spectrum of incident neutrons $G(E)$ modified by the energy dependence of the detection efficiency $\epsilon(E)$. Thus

$$\left(\sigma(\theta)\right)_{\text{pred.}} = \frac{\int_{E_{min}}^{E_{max}} \sigma(\theta,E) G(E)\, \epsilon(E)\, dE}{\int_{E_{min}}^{E_{max}} G(E)\, \epsilon(E)\, dE}$$

It is not necessary to account for any change in energy of the neutrons upon

being scattered, for the lightest nucleus employed is Al, and the scattering is confined to small angles. The averaging is accomplished by graphical integration using information on the neutron energy spectrum previously mentioned, and some approximate experimental data, supplemented by theory,[6,7] on the $C^{12}(n,2n)C^{11}$ cross section and its variation with energy.

The functions (13) and (15) are indistinguishable within the limits of accuracy needed in this comparison, so (15) has been employed. The principal effect of the averaging process just described is to increase the contribution in the vicinity of the first root of the Bessel Function above that obtained from a pure spectrum of 84 Mev neutrons.

C. Comparison of Observations with Theory

By integration of the differential scattering cross section as given by (13) the elastic scattering cross section is obtained:

$$\sigma_s = 2\pi \int_\theta^\pi \frac{1}{4k^2}\left[\sum_{\ell=0}^{\ell=kR} (2\ell + 1)\, P_\ell\, (\cos\theta)\right]^2 \sin\theta d\theta$$

$$= \pi\, (R + \frac{1}{k})^2 = \pi R'^2 . \qquad (16)$$

An experimental value for σ_s will, by use of (16), allow determination of R', which, in turn, may be used in (15) to construct angular distribution curves appropriate to the opaque model for comparison with the shapes of the experimental distributions.

This comparison is shown in Figure 5. The dashed curves are the result of determining R' from the values of σ_s' displayed in Table III; and the dotted curves result from using $(\sigma_s' - \sigma_2)$ for determining R'. In each case the distribution given by (15) has been modified as in the preceding Section B to account for the energy spread of the neutrons.

In view of Sections V, B and C, and Equation (16), we should actually

determine R' from $\sigma_s = \sigma_s' - \sigma_2 + \sigma_1 = \pi(R')^2$. The value of σ_1 is very small in the cases of Cu and Pb, but may be comparable with σ_2 in the case of Al as shown in the experimental results of Section V-C. These facts are consistent with the agreement of the dotted curves with datum points for Pb and Cu, while for Al the points are closer to the dashed curve computed from σ_s'.

To be consistent, one should subtract from the datum point ordinates the values of the differential cross sections for inelastic collisions delivering detectable neutrons, estimated in the manner described in Section V-B. But this does not significantly alter the positions of the points except at very wide angles where the datum point accuracy does not warrant such correction.

A calculation of the angular distribution has also been made on the basis of the "transparent" model of Fernbach, Serber, and Taylor.(3) This model assumes for nuclear matter an absorption coefficient and an index of refraction. The radius of an individual nucleus according to this scheme can be represented by $r_0A^{1/3}$. In the case previously described, based on the total cross section measurements of Cook, McMillan, Peterson and Sewell, the radius of the nucleus is given by $1.37\ A^{1/3} \times 10^{-13}$ cm when K (the absorption coefficient) is chosen as 2.2×10^{12} cm^{-1} and k_1 (the increase of the propagation constant of the neutron wave upon entering the nucleus) as 3.3×10^{12} cm^{-1}.

The angular distributions determined with these constants yield the curves shown in Figure 6. The theoretical curves are noticeably lower than the experimental values in the forward direction, but fit comparatively well at other angles. The Bessel function obtained from the opaque model on the other hand fits better in the forward direction but not as well at larger angles.

Figure 7 shows the theoretical curve for σ_a/σ_t as a function of nuclear radius. The experimental points are taken from the attenuation data obtained from the poor geometry experiment.

Curve A is calculated with the above mentioned constants, Curve B with constants that fit this attenuation data better. Neither the angular distribu-

tion nor the total cross sections are very sensitive to changes in the value of the absorption constant, whereas the absorption cross section is a function of KR only. Hence a poor geometry attenuation experiment can be used to make a more critical determination of K. In this case $K = 3.0 \times 10^{12}$ cm^{-1} shows better agreement with the experimental results. It should be mentioned that with this value of K, the value of r_0 necessary to give the best fit for the total cross sections is 1.39×10^{-13} cm.

In Figure 7 the experimental values have not been corrected for the scattering beyond the maximum angle used. The only appreciable scattering beyond θ_{max} seems to be that for aluminum. Such correction would reduce the ratio σ_a/σ_t and bring the experimental point closer to the theoretical curve.

VII. Acknowledgments

The authors wish to express their appreciation to Professor E. O. Lawrence for his interest in this work. We are indebted to Professor E. McMillan for originally suggesting the problem and for helpful discussions. We also wish to thank Mr. James Vale and the cyclotron operating crew for their valuable assistance.

This paper is based on work performed under the auspices of the Atomic Energy Commission.

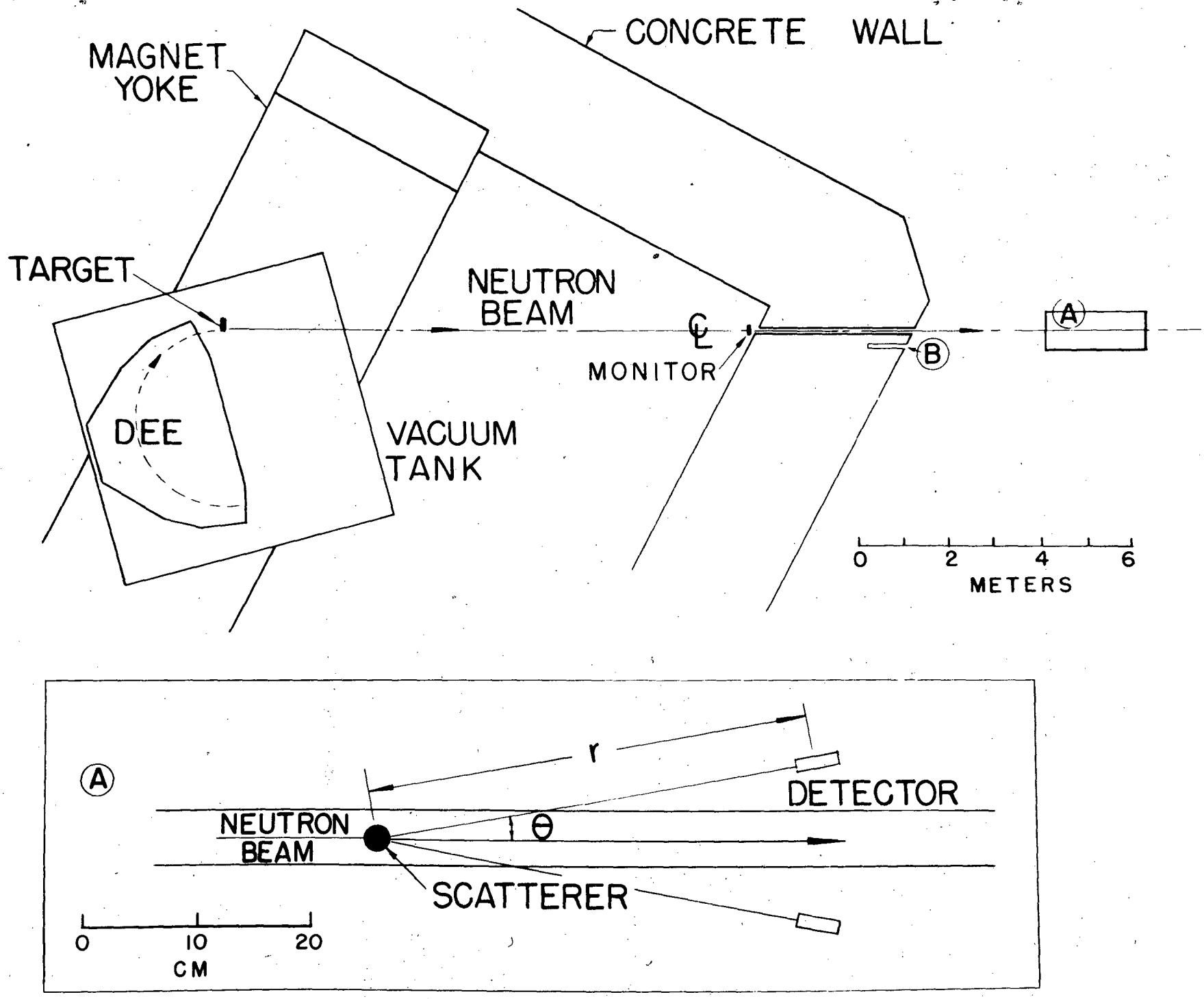

FIG. I PLAN VIEW OF EXPERIMENTAL ARRANGEMENT.

07 579

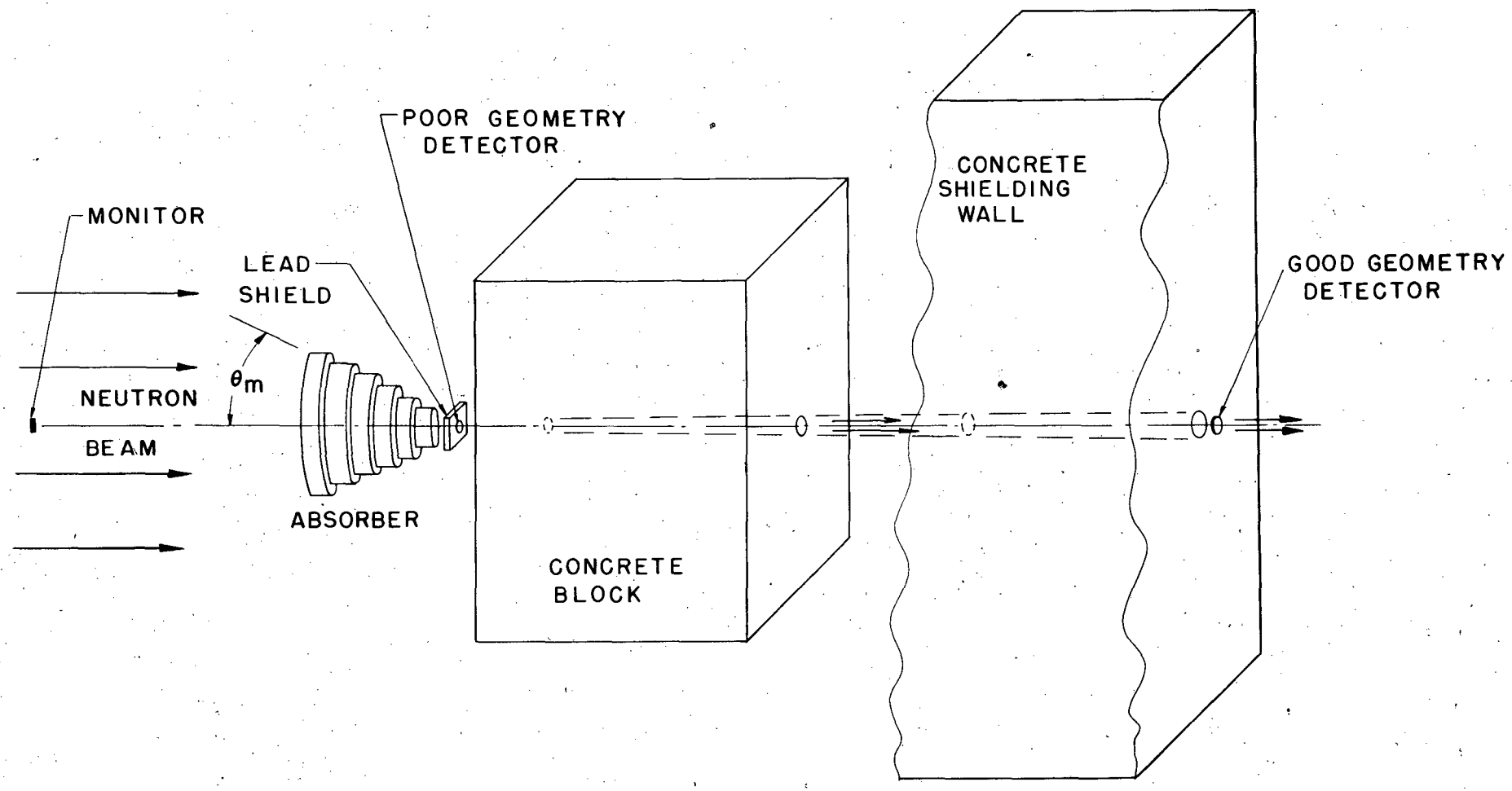

FIG. 2

SCHEMATIC DRAWING OF APPARATUS FOR ATTENUATION EXPERIMENTS

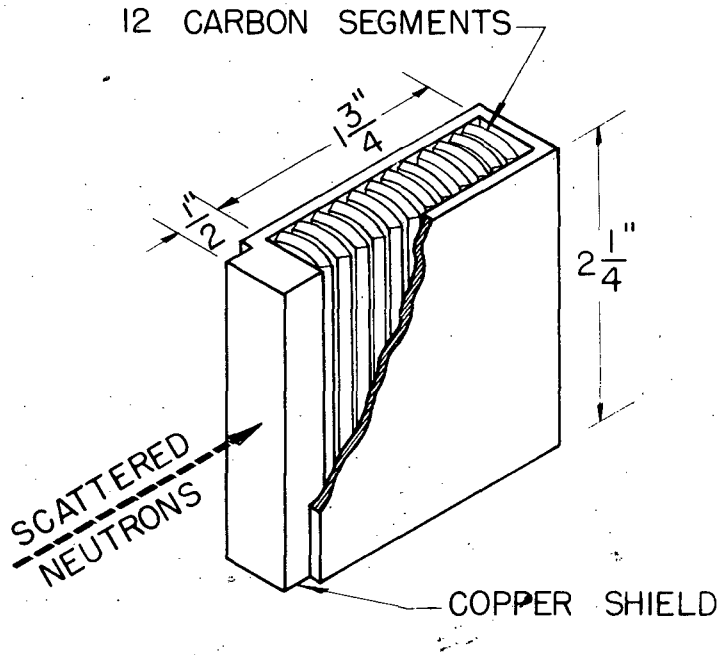

CARBON DETECTOR

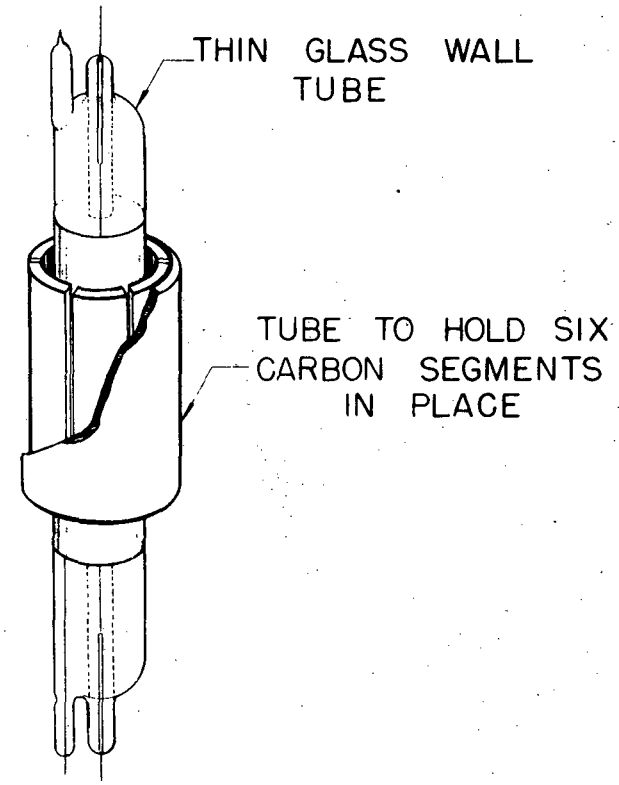

CARBON SEGMENTS IN POSITION TO BE COUNTED

FIG. 3

DETECTOR AND DETECTOR COUNTING ARRANGEMENT

OZ 580

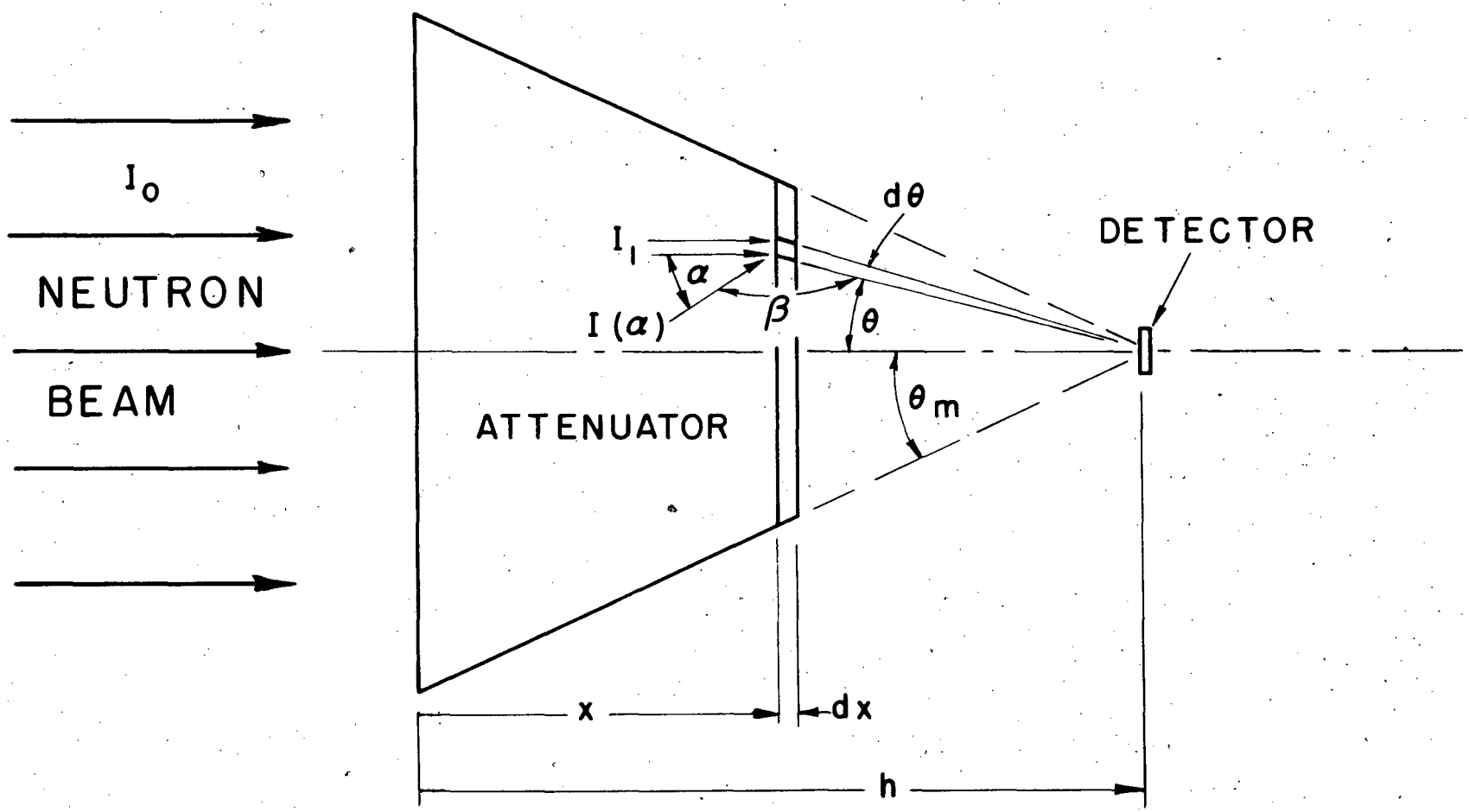

FIG. 4
GEOMETRY OF ATTENUATION EXPERIMENT

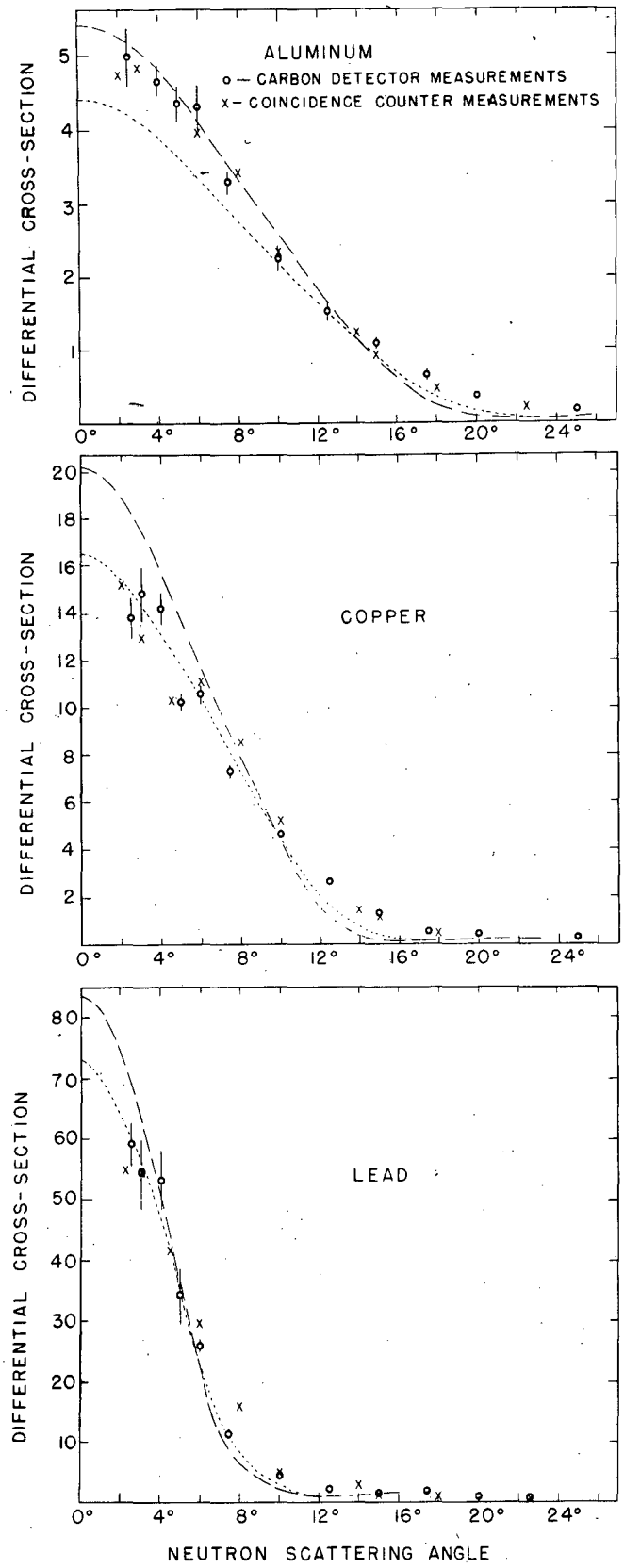

FIG. 5. DIFFERENTIAL SCATTERING CROSS SECTIONS IN UNITS OF 10^{-24} cm^2 PER STERADIAN. THE DASHED AND DOTTED CURVES SHOW EXPECTED PATTERNS FROM OPAQUE NUCLEU WITH CROSS SECTIONS σ_s' AND $(\sigma_s' - \sigma_2)$ RESPECTIVELY. (SEE SECTION VI-C)

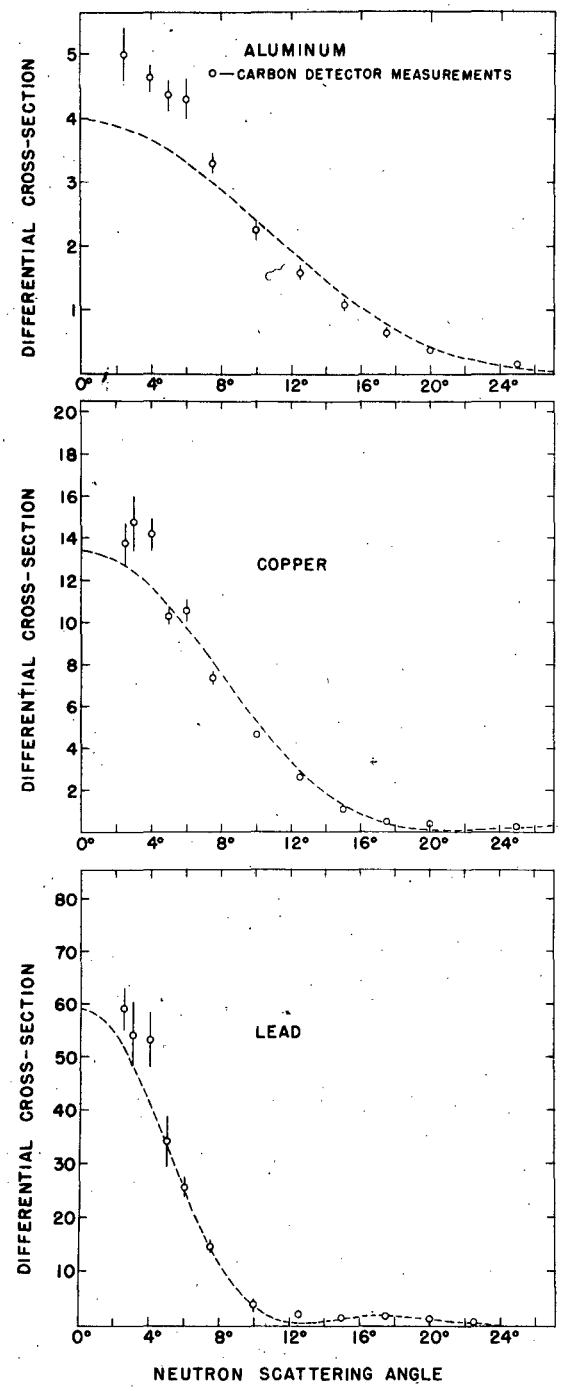

FIG. 6 COMPARISON OF EXPERIMENTAL DIFFERENTIAL CROSS SECTIONS WITH THOSE CALCULATED FROM TRANSPARENT MODEL THEORY. (UNITS SAME AS IN FIG. 5).

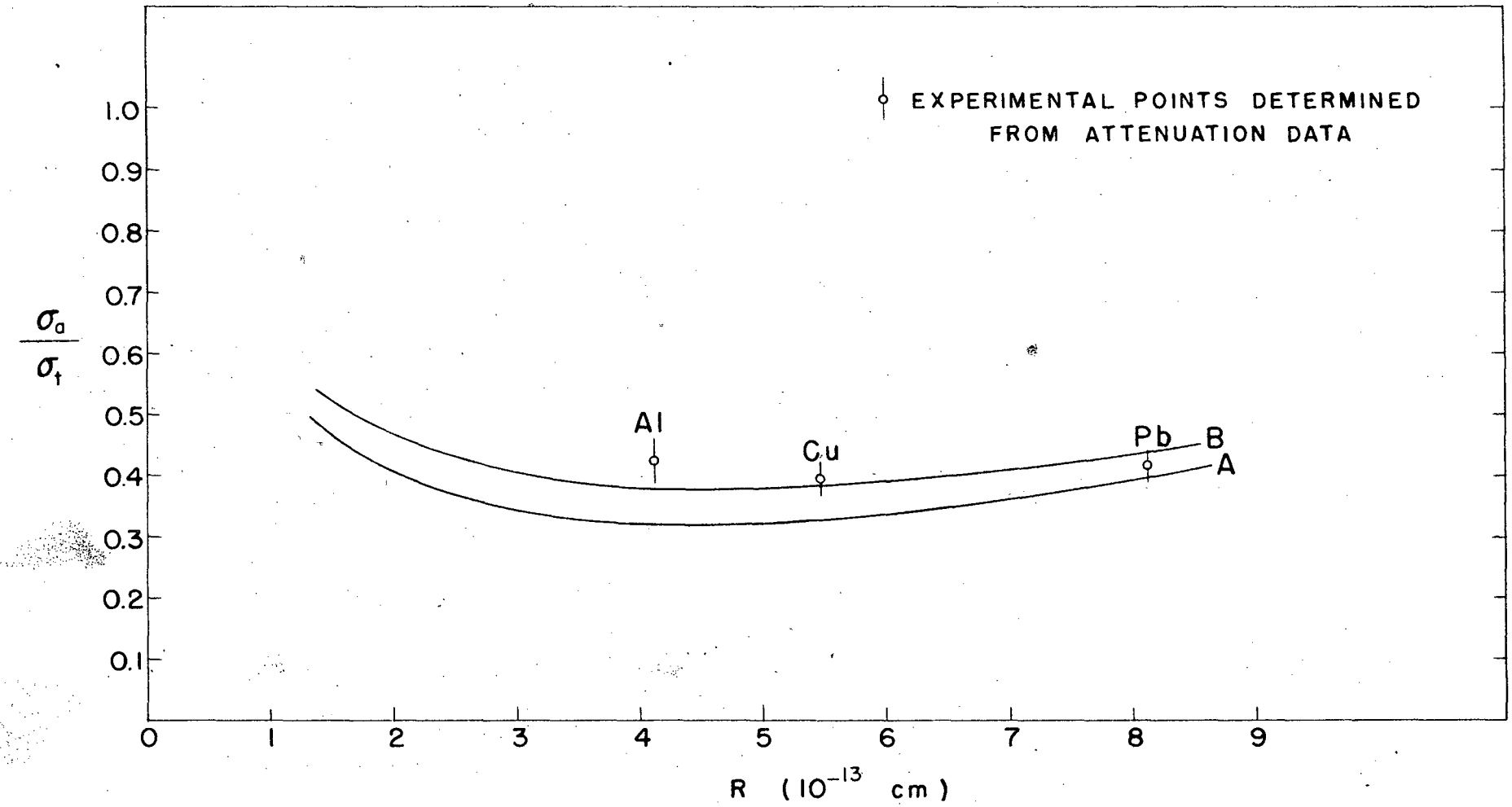

THEORETICAL CURVES FOR σ_a / σ_t VS. R ($R = 1.37 A^{1/3} \times 10^{-13}$ cm)

A: $K = 2.2 \times 10^{12}$ cm^{-1}, $K_1 = 3.3 \times 10^{12}$ cm^{-1}

B: $K = 3.0 \times 10^{12}$ cm^{-1}, $K_1 = 3.3 \times 10^{12}$ cm^{-1}

14159-1

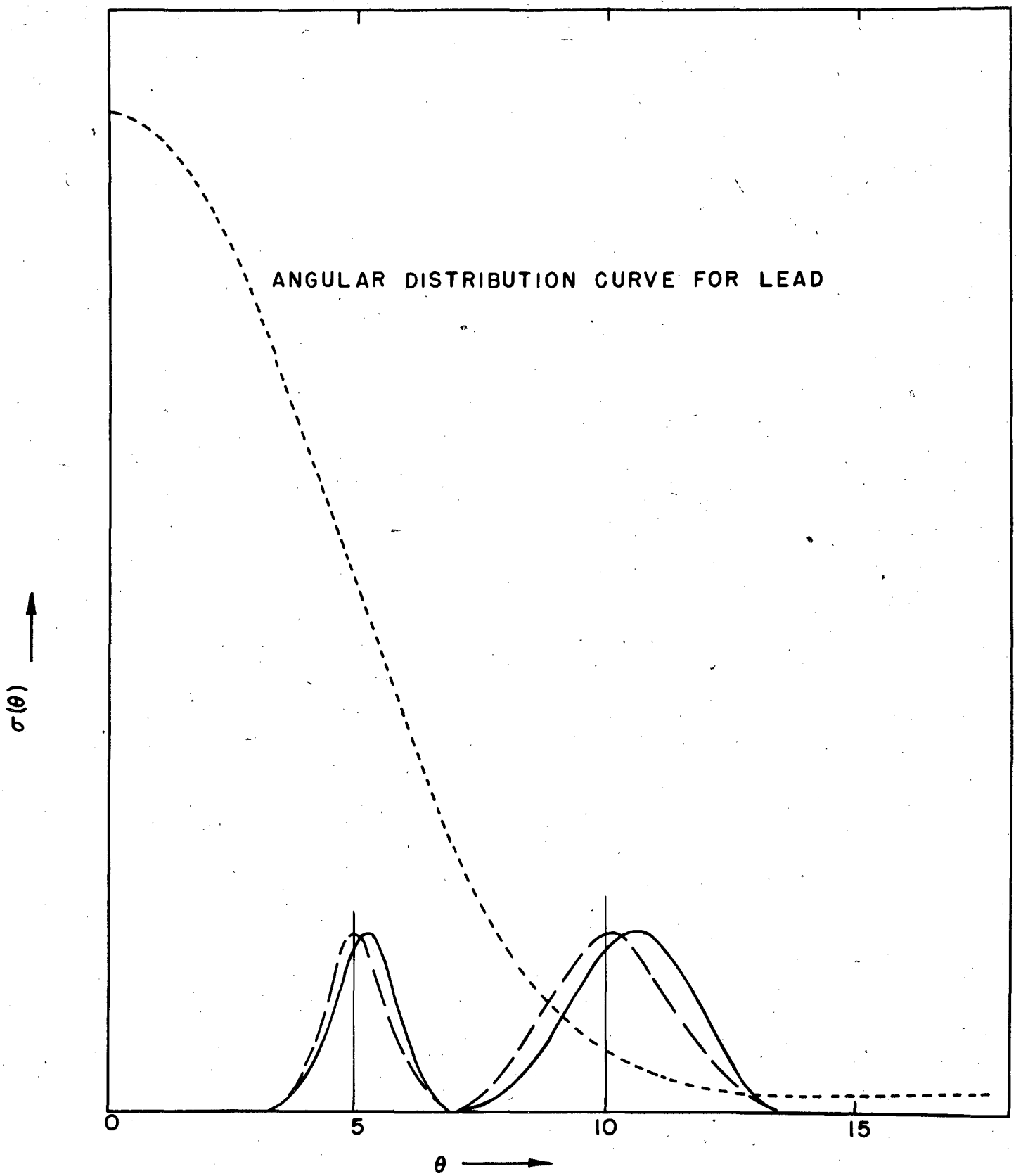

FIG. 6. ANGULAR RESOLUTION. THE SOLID BELL-SHAPED CURVES SHOW THE DETECTION DISTRIBUTION FOR TWO TYPICAL DETECTOR POSITIONS IN THE MEASUREMENT OF THE ANGULAR DISTRIBUTION FROM THE LEAD SCATTERER (5° AT 65 cm. AND 10° AT 34cm). WHEN THESE ARE MULTIPLIED BY THE DOTTED CURVE WHICH HAS THE FORM OF THE ANGULAR DISTRIBUTION FOR LEAD WE OBTAIN THE EFFECTIVE DETECTION DISTRIBUTION SHOWN AS DASHED CURVES

Incorrectly Stamped

~~SECRET~~

~~UNCLASSIFIED~~